BBA - Molecular Basis of Disease 1870 (2024) 167283

Contents lists available at ScienceDirect

BBA - Molecular Basis of Disease

journal homepage: www.elsevier.com/locate/bbadis

Oral β-RA induces metabolic rewiring leading to the rescue of diet-induced obesity

María Elena Díaz-Casado [a,b,c], Pilar González-García [a,b,c], Sergio López-Herrador [a,b], Agustín Hidalgo-Gutiérrez [a,b,d], Laura Jiménez-Sánchez [c], Eliana Barriocanal-Casado [d,e], Mohammed Bakkali [f], Chris H.A. van de Lest [g], Julia Corral-Sarasa [c], Esther A. Zaal [g], Celia R. Berkers [g], Luis C. López [a,b,c,h,*]

[a] Departamento de Fisiología, Facultad de Medicina, Universidad de Granada, 18016 Granada, Spain
[b] Instituto de Biotecnología, Centro de Investigación Biomédica, Universidad de Granada, 18016 Granada, Spain
[c] Instituto de Investigación Biosanitaria Ibs. Granada, 18016 Granada, Spain
[d] Department of Neurology, Columbia University Medical Center, New York, NY 10032, USA
[e] GENYO, Centre for Genomics and Oncological Research, Genomic Medicine Department, Pfizer-University of Granada-Andalusian Regional Government, 18016 Granada, Spain
[f] Departamento de Genética, Facultad de Ciencias, Universidad de Granada, 18071 Granada, Spain
[g] Division of Cell Biology, Metabolism & Cancer, Department of Biomolecular Health Sciences, Faculty of Veterinary Medicine, Utrecht University, 3508 TD Utrecht, the Netherlands
[h] Centro de Investigación Biomédica en Red Fragilidad y Envejecimiento Saludable (CIBERFES), 18016 Granada, Spain

ARTICLE INFO

Keywords:
Mitochondria
Coenzyme Q
Diet-induced obesity
NAFLD
MASLD
Pharmacological therapy
Preclinical study

ABSTRACT

Obesity represents a significant health challenge, intricately linked to conditions such as type II diabetes, metabolic syndrome, and hepatic steatosis. Several existing obesity treatments exhibit limited efficacy, undesirable side effects or a limited capability to maintain therapeutics effects in the long-term. Recently, modulation Coenzyme Q (CoQ) metabolism has emerged as a promising target for treatment of metabolic syndrome. This potential intervention could involve the modulation of endogenous CoQ biosynthesis by the use of analogs of the precursor of its biosynthesis, such as β-resorcylic acid (β-RA). Here, we show that oral supplementation with β-RA, incorporated into the diet of diet-induced obese (DIO) mice, leads to substantial weight loss. The anti-obesity effects of β-RA are partially elucidated through the normalization of mitochondrial CoQ metabolism in white adipose tissue (WAT). Additionally, we identify an HFN4α/LXR-dependent transcriptomic activation of the hepatic lipid metabolism that contributes to the anti-obesity effects of β-RA. Consequently, β-RA mitigates WAT hypertrophy, prevents hepatic steatosis, counteracts metabolic abnormalities in WAT and liver, and enhances glucose homeostasis by reducing the insulin/glucagon ratio and plasma levels of gastric inhibitory peptide (GIP). Moreover, pharmacokinetic evaluation of β-RA supports its translational potential. Thus, β-RA emerges as an efficient, safe, and translatable therapeutic option for the treatment and/or prevention of obesity, metabolic dysfunction-associated steatotic liver disease (MASLD).

1. Introduction

Obesity is defined as abnormal or excessive fat accumulation that presents a great risk to health. The incidence of diet-induced obesity is continuously increasing in developed countries, and it is linked to an increased risk of developing non-transmissible diseases, such as insulin resistance, type II diabetes, metabolic dysfunction-associated steatotic liver disease (MASLD), metabolic syndrome, cardiovascular diseases, some types of cancer, and disorders of the locomotor system, among others [1]. Therefore, obesity is a serious and growing health problem worldwide [2].

Although the main strategies used for the treatment of obesity focus on reducing body weight, this effect is frequently not due to an exclusive reduction in the content of white adipose tissue (WAT) [2,3]. Moreover,

* Corresponding author at: Departamento de Fisiología, Facultad de Medicina, Universidad de Granada, 18016 Granada, Spain.
E-mail address: luisca@ugr.es (L.C. López).

https://doi.org/10.1016/j.bbadis.2024.167283
Received 25 March 2024; Received in revised form 23 May 2024; Accepted 31 May 2024
Available online 6 June 2024

some drugs used for the treatment of obesity, insulin resistance, type II diabetes, metabolic syndrome or MASLD frequently show heterogeneous results in the population, low efficiency, side effects and/or a limited capability to maintain therapeutics effects in long-term [2,3]. Therefore, there is still a need to identify novel strategies to efficiently treat obesity, and its medical consequences. In this context, therapeutic mechanisms targeting WAT and/or utilizing fatty acids may exhibit high efficacy with minimal adverse effects.

The mechanisms by which obesity can induce insulin resistance, type II diabetes and metabolic syndrome are heterogenous, including the deregulation of endocrine factors, the induction of inflammation, the disruption of the neural circuits of food intake or the presence of cell-intrinsic mechanisms. Cell-intrinsic mechanisms involve ectopic fat storage, ER stress, mitochondrial dysfunction, and oxidative stress [4]. Mitochondrial dysfunction contributes to ectopic fat accumulation, deregulation of glucose metabolism and increased generation of reactive oxygen species (ROS). Recently, a down-regulation of the mitochondrial Coenzyme Q (CoQ) biosynthetic pathway and, consequently, a decrease in the levels of CoQ were reported in WAT and muscle from a mouse model of diet-induced-obesity (DIO) and WAT from humans with insulin-resistance [5]. As an essential component of the mitochondrial respiratory chain, CoQ links ATP production to different metabolic pathways via the Q-junction, while also serving as an important endogenous antioxidant. Consequently, the decrease in CoQ levels in WAT and muscle was identified as a cause of mitochondrial dysfunction and increased oxidative stress, leading to the induction of insulin resistance [5].

The link between CoQ deficiency, obesity and insulin resistance opens a potential therapeutic target focused on the modulation of CoQ metabolism in the affected tissues. Interestingly, β-resorcylic acid (β-RA), a natural phenolic compound with an analog structure to 4-hydroxybenzoic acid, the precursor for CoQ biosynthesis, decreased the content of WAT and overall body weight in mice fed a standard chow diet, although the mechanisms underlying this effect remain unclear. [6,7]. β-RA has also shown clear therapeutic benefits in different mouse models of primary CoQ deficiency by interfering in the CoQ biosynthetic pathway [6–11]. However, whether β-RA can be effective in reducing the content of WAT in specific models of obesity remains largely

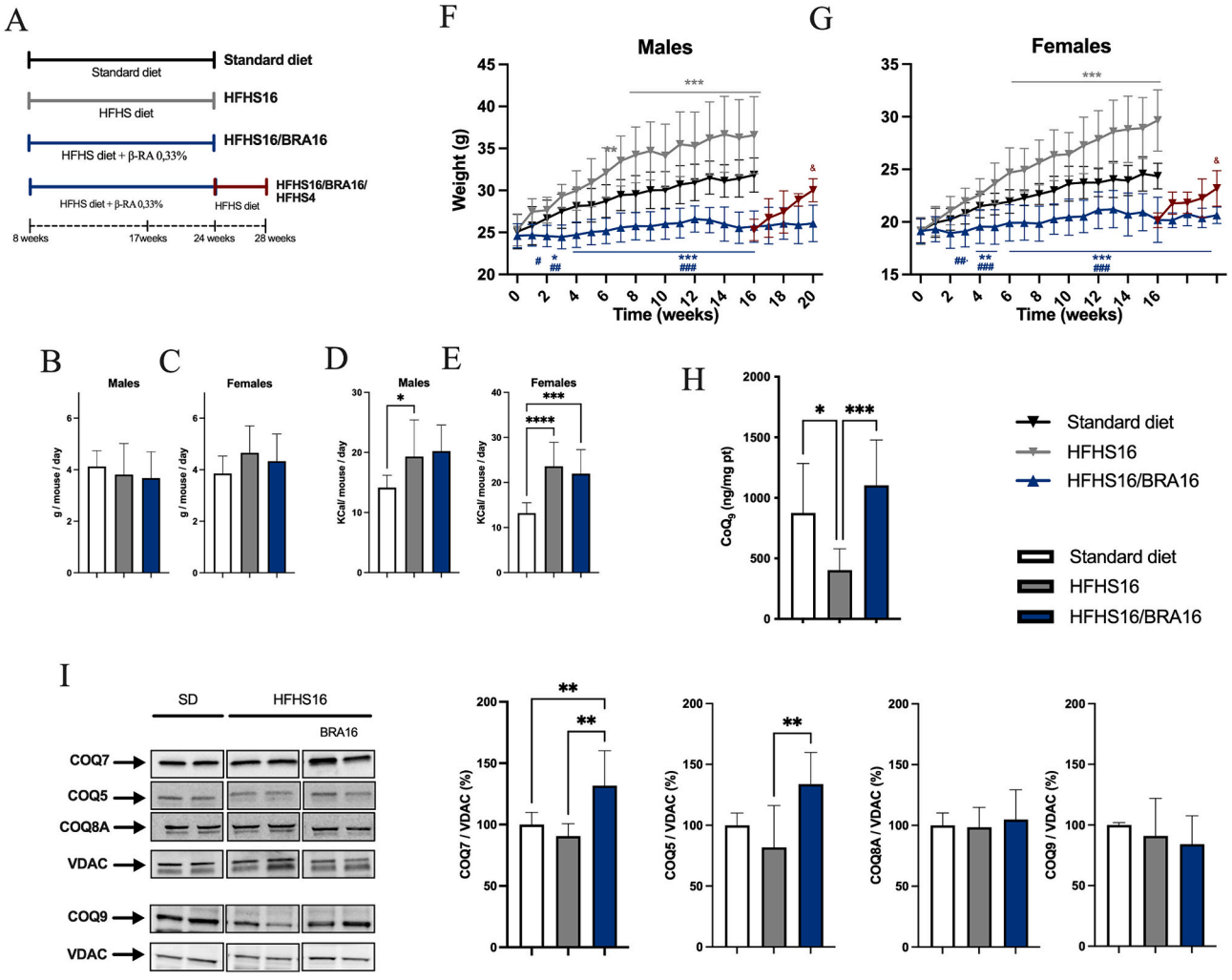

Fig. 1. Effect of β-RA treatment on body weight and mitochondrial CoQ biosynthesis in DIO mice. (A) Schematic figure of the experimental design for β-RA treatment in DIO mice. (B, C) Daily food intake in male (B) and female (C) mice ($n = 10$ for each group). (D,E) Daily caloric intake in male (D) and female (E) (n = 10 for each group). (F–G) Body weight of male (F) and female (G) mice on standard diet, HFHS diet, HFHS diet +0.33 % β-RA at different times ($n = 23$ in control group, $n = 17$ in HFHS16 group, n = 17 in HFHS16/BRA16 group in males; $n = 27$ in control group, $n = 16$ in HFHS16 group and n = 16 in HFHS16/BRA16 group). * $p < 0.05$, ** $p < 0.01$, *** $p < 0.001$, differences versus standard diet group; # $p < 0.05$, ## $p < 0.01$, ### $p < 0.001$, differences versus HFHS16 group; & $p < 0.05$, differences versus HFHS16/BRA16 group. (H) Levels of mitochondrial CoQ_9 in WAT (n = 10 for each group). (I) Representative images of Western blots of the CoQ biosynthetic proteins and the quantification of the protein bands COQ7, COQ5, COQ8A and COQ9 ($n = 5$ for each group). Data are expressed as mean ± SD. * $p < 0.05$, ** $p < 0.01$, *** $p < 0.001$, differences versus standard diet group; significance was assessed by one-way ANOVA tests with Tukey's post hoc test or Sídák's multiple comparisons test as appropriate multiple comparisons test. Samples used in the standard diet and HFHS groups were also used in the Fig. S4.

unknown. Moreover, its metabolization and pharmacokinetics have not been evaluated.

Here, we show that oral β-RA induces weight loss by normalizing CoQ biosynthesis in mitochondria of WAT in diet-induced obese (DIO) mice. Additionally, we observe a transcriptomic activation of hepatic lipid metabolism. As a result, β-RA reduces content of WAT and mitigates the morphological features of MASLD, counteracting metabolic disarrangements in both WAT and liver, and ameliorating insulin resistance.

2. Results

2.1. β-RA rescues the DIO phenotype by normalizing CoQ biosynthesis in WAT

Following previous studies, C57BL/6J wild-type mice were fed with a high-fat high-sucrose (HFHS) diet for 16 weeks (HFHS16), and β-RA was incorporated into the HFHS diet (HFHS16/BRA16) at a concentration of 0.33 % (*w*/w) [7,8,12]. This provides a dose of 0.3–0.7 g/kg b.w./day, considering the animal food intake, which is similar in all groups (Fig. 1A–C). Therefore, there is an increase in caloric intake in DIO mice, compared to animals fed in standard diet (Fig. 1D–E). As expected, HFHS16 induces an increase in body weight in both males and females, compared to animals fed with standard diet (Fig. 1F–G). Remarkably, the body weight in HFHS16/BRA16 mice is significantly lower than those in animals fed with either HFHS16 or standard diet, in both males and females (Fig. 1F–G). The maximal body weight reached in HFHS16/BRA16 mice is about 26 g in males and 20 g in females, representing a reduction of 29 % in males and 33 % in females, compared to the HFHS16 mice. The prevention in body weight gain is reversible since the effect disappears rapidly after suppressing β-RA therapy in the animals fed with HFHS diet (HFHS16/BRA16/HFHS4), in both males and females (Fig. 1A, F–G). β-RA treatment causes similar effect on reducing weight gain in the nicotinamide nucleotide transhydrogenase knockout (NNT^{KO}) C57BL/6 J mice (Fig. S1A–C), which have been identified as more prone to the obese phenotype [13]. Moreover, the reduced body weight in mice after β-RA treatment is mainly caused by the prevention and reduction in the accumulation of WAT (Figs. S2-B; S1D–E), while still preserving the weight of skeletal muscle (Figs. S2C–D; S1F–G).

Since an altered mitochondrial CoQ biosynthetic pathway, and the subsequent secondary CoQ deficiency, has been proposed as key inducer of obesity [5,14], and because β-RA supplementation has been reported to modulate CoQ biosynthesis in models of primary CoQ deficiency [6,8,15], we evaluated whether the anti-obesity effects of the β-RA in the DIO model could be explained by its action in the CoQ biosynthetic pathway. To do this, we first measured mitochondrial CoQ_9 content in WAT, skeletal muscle and liver. As expected, the HFHS diet decreases CoQ_9 levels in mitochondria in WAT (Fig. 1H) but not in skeletal muscle or liver (Fig. S3A and C). Remarkably, β-RA therapy normalizes the mitochondrial CoQ_9 levels in WAT (Fig. 1H). To check whether the effects on CoQ levels are due to changes in the mitochondrial CoQ biosynthetic pathway, we quantified the levels of four key proteins involved in CoQ biosynthesis. A trend toward decreased levels of COQ7 and COQ5 are observed in WAT from HFHS mice, compared to mice fed with the standard diet (Fig. 1I). Importantly, β-RA therapy increases the steady-state levels of COQ7 and COQ5 in WAT and skeletal muscle, although other proteins, i.e., COQ8A and COQ9, remain unchanged in those tissues and in the liver (Figs. 1I; S3B–D).

Since some analogs of β-RA, e.g., 4-hydroxybenzoic acid (4HB) and vanillic acid (VA), could also interfere with the mitochondrial CoQ metabolism [11,16,17], we also tested the capability of those compounds to increase the levels of mitochondrial CoQ_9 and decrease the content of WAT. Also, we compared the results with those obtained in an experimental group based on exogenous CoQ_{10} supplementation. Comparing the three compounds, only 4HB has a mild effect in preventing the increase in body weight, both in males and females (Fig. S4A–B) and only reduces WAT content (Fig. S4E–H), without affecting the food intake (Fig. S4C–D).

Accordingly, VA (HFHS16/VA16) nor CoQ_{10} (HFHS16/CoQ16) have any effects on the levels of CoQ_9 in WAT, whereas 4HB (HFHS16/4HB16) slightly increases mitochondrial CoQ_9 levels in WAT (Fig. S5A), but not in skeletal muscle or liver (Fig. S5B,C). However, the levels of the CoQ biosynthetic proteins do not change with any treatment in WAT, skeletal muscle or liver, except for an increase of COQ5 with VA in skeletal muscle (Fig. S5A–F). Together, these data confirm that the modulation of CoQ metabolism in WAT could be a therapeutic target for obesity.

2.2. β-RA induces a transcriptomic activation of hepatic lipid metabolism

To explore any additional anti-obesity mechanism of β-RA, we next performed transcriptomics analyses in three tissues involved in the control of lipid and carbohydrate metabolism, i.e., the liver (Fig. 2A–J), WAT (Fig. S6A,C) and skeletal muscle (Fig. S6B,D) (Supporting information). These analyses were performed in already obese mice (HFHS11) and mice that were treated for two weeks with β-RA, once they acquired the obese phenotype (HFHS11/BRA2) and, therefore, at the moment they were actively losing weight (Fig. 2A–C). Both groups were compared to aged-match mice fed under standard diet. While WAT and skeletal muscle experiences only minor changes in gene expression, without changes induced by β-RA (Fig. S6A–D), the livers undergo important transcriptomics modifications in all three experimental groups. The livers of HFHS11 mice exhibit 429 differentially expressed genes compared to the liver of animals fed with standard diet; the livers of HFHS11/BRA2 mice show 1088 differentially expressed genes compared to the livers of HFHS11 mice; and the livers of HFHS11/BRA2 mice show 3842 differentially expressed genes compared to the livers of animals fed with standard diet. Analyses of canonical pathways revealed that HFHS diet activates fatty acids β oxidation and triacylglycerol degradation, while inhibits cholesterol biosynthesis and signaling pathways controlled by the receptors LXR-RXR and PXR-RXR, both involved in the regulation of hepatic lipid metabolism (Fig. 2D–E). β-RA therapy further activates fatty acids β oxidation, triacylglycerol degradation and signaling pathways controlled by the receptors LXR-RXR, while additionally inhibiting cholesterol biosynthesis (Fig. 2D–E). Analyses of the potential upstream regulators revealed common and different patterns in HFHS11 and HFHS11/BRA2 mice (Fig. 2H–I). Interestingly, genes controlled by the hepatocyte nuclear factor 4 alpha (HNF4α), a transcription factor that controls the expression of downstream genes that are important in multiple aspects of hepatic metabolism [18], are predominantly unaltered or downregulated under HFHS diet, while β-RA therapy induces an activation of HNF4α regulation (Fig. 2H–J). These results suggest that LXR-RXR and HNF4α may be involved in the induction of lipid catabolism in the liver under β-RA therapy.

2.3. β-RA prevents MASLD and WAT hypertrophy in DIO mice

The profound changes in the hepatic transcriptome are congruent with the striking modification of the hepatic function and phenotype. Moreover, obesity is the greatest risk factor for developing MASLD. Accordingly, the livers of mice after 16 weeks on the HFHS diet show features of steatosis under hematoxylin & eosin (H&E) and oil-red (ORO) stains (Fig. 3A–G). These features of steatosis are not present in the β-RA treated group, since the lipid content in the liver is significantly reduced, reaching values like those of the control group. With the related compounds, only 4HB decreases the lipid content in the liver (Fig. S7). The observed fat profiles of the livers in the three experimental groups are consistent with the increased levels of hepatic triglycerides in HFHS16 mice and the normalization induced by β-RA therapy (Fig. 3H). Furthermore, the livers of HFHS16 mice show alterations in several

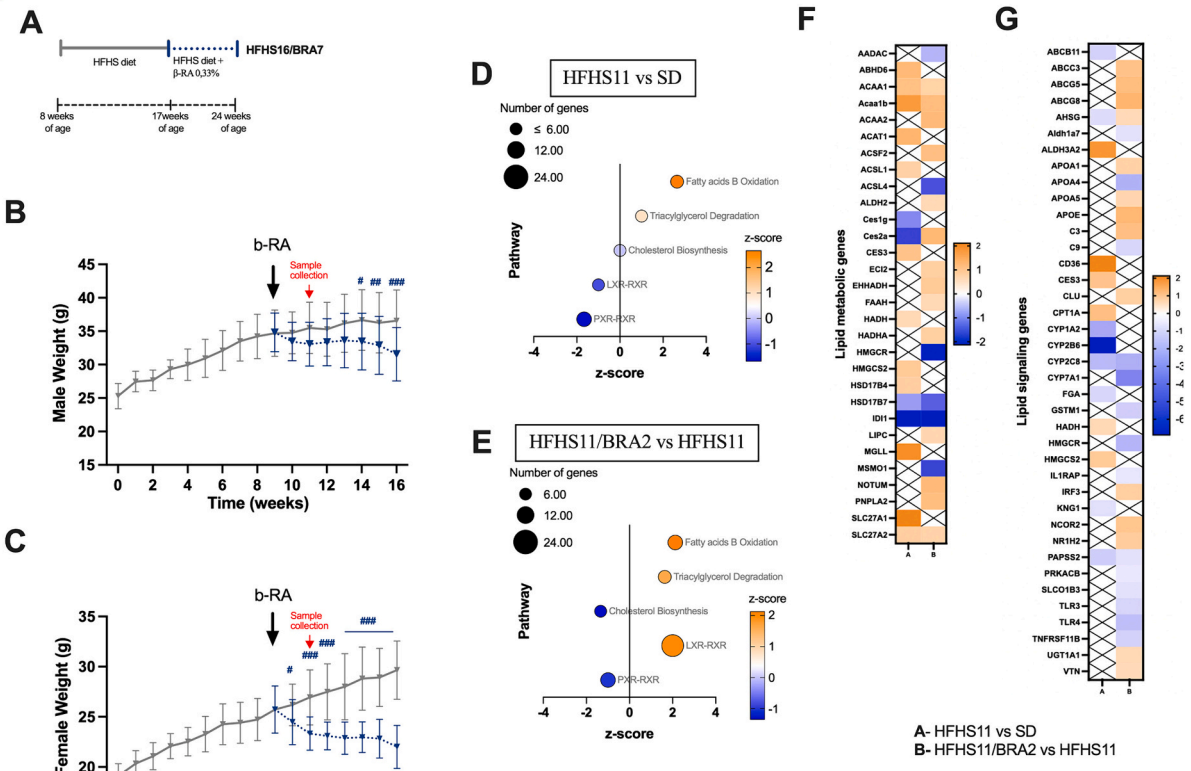

(caption on next page)

Fig. 2. Profile of hepatic gene expression. (A) Schematic figure of the experimental design for β-RA treatment in DIO mice. (B, C) Body weight of male (B) and female (C) mice on HFHS diet and HFHS diet +0.33 % β-RA at 9 weeks on HFHS (n = 16 for HFHS16 group and n = 10 for HFHS16/BRA7 group in males; $n = 18$ for HFHS16 and $n = 9$ for HFHS16/BRA7 group in females). # $p < 0.05$, ## $p < 0.01$, ### $p < 0.001$, differences versus HFHS16 group. (D–E) Representation of the canonical pathways altered by HFHS diet (D) and by the treatment with β-RA (E). z-Score indicates a predicted activation or inhibition of a pathway/gene, where a negative z value connotes an overall pathway's inhibition (represented in blue), and a positive z value connotes an overall pathway's activation (represented in orange). (F–G) Representative heatmap of the expression level of the genes involved in lipid metabolism and that appear significantly altered by HFHS diet and by the treatment with β-RA. Orange indicates overexpression of the indicated gene, and blue downregulation of the indicated gene. A Crossed box indicates that the expression of indicated gene was not statistically different in that comparison. (H–I) Representation of the upstream regulators that are predicted to be involved in the alterations induced by HFHS diet (H) and by the treatment with β-RA (I). z-score indicates a predicted activation or inhibition of a pathway/gene, where a negative z value connotes an overall pathway's inhibition (represented in blue), and a positive z value connotes an overall pathway's activation (represented in orange). (J) Representative heatmap of the expression levels of genes regulated by HNF4α. Orange indicates overexpression of the indicated gene, and blue downregulation of the indicated gene. A Crossed box indicates that the expression of indicated gene was not statistically different in that comparison.

metabolic pathways, i.e., the urea cycle (Fig. 3I) and pyrimidine metabolism (Fig. 3K), especially in the levels of uracil. The treatment with β-RA reverses some of the metabolic perturbation associated with the HFHS diet, indicating a partial normalization of the hepatic metabolic functions following the decrease in steatosis (Fig. 3I–K).

NALFD and increased WAT volume are frequently associated, and both are linked to obesity. In adult animals and humans, voluminal expansion of WAT is caused by hypertrophy of adipocytes. As such, it was shown that the increased WAT content of mice fed with a high-fat diet was associated with larger adipocyte size (Cummins et al., 2014), a hallmark of obesity that is absent in mice treated with β-RA. Specifically, morphologic analysis of epididymal WAT shows hypertrophied adipocytes, with lower number per area and increased size, in HFHS16 mice, compared to animals fed with standard diet (Fig. 4A–E). β-RA treatment shows a two-fold decrease in adipocyte size and an increase in adipocyte number per area, when compared with the HFHS16 group (Fig. 4A–E). Other related compounds do not impact on the size and number of the adipocytes per area (Fig. S8A–C).

Since obesity is associated with metabolic rewiring of WAT [19], we also performed a metabolic analysis of the WAT in the different experimental groups. In HFHS16 mice, the level of lactate and sedoheptulose-7P, intermediate of the pentose phosphate pathway, are decreased compared to the mice fed with the standard diet or β-RA supplementation, respectively (Fig. 4F). Moreover, levels of some glycolytic-related intermediates are altered. Specifically, the amount of 2P-glycerate is lower in HFHS16 mice compared to those in the animals fed with the standard diet (Fig. 4F). Also, the levels of the TCA cycle intermediates alpha-ketoglutarate and malate are higher in HFHS16 mice (Fig. 4F), indicating higher energy metabolism or utilization of acetyl-CoA for fatty acid synthesis. β-RA supplementation counterbalances the deviations of the aforementioned molecules caused by HFHS diet, most likely due to normalization of the TCA cycle (Fig. 4F–G). Together, these data indicate that β-RA decreases the hypertrophy of adipocytes by reducing fatty acid synthesis and normalizing WAT metabolism.

2.4. *β-RA reduces hyperlipidemia and alleviates HFHS-induced insulin resistance*

The obese phenotype induced by HFHS diet is also reflected by hypertriglyceridemia, hypercholesterolemia, hyperglycemia and insulin resistance, in both males (Fig. 5A, C, E, G, I, K) and females (Fig. 5B, D, F, H, J, L). β-RA treatment induces a decrease in circulating triglycerides, total cholesterol and fasting glucose in HFHS16/BRA16, compared to HFHS mice, with a more pronounced effect in males (Fig. 5A, C, E, G, I, K) than in females (Fig. 5B, D, F, H, J, L). The glycemic control was assessed by intraperitoneal glucose tolerance testing (GTT), which shows a marked improvement of HFHS-induced glucose intolerance in male β-RA-treated mice (Fig. 5G, I), but not in females (Fig. 5H, J). Further evaluation of insulin resistance by intraperitoneal insulin tolerance testing (ITT) reveals an improvement in glucose clearance in HFHS16/BRA16 mice relative to HFHS mice (Fig. 5K–L). With the related molecules the results are consistent with the genetic, metabolic and morphological data, since only 4HB slightly decreases the insulin resistance (Fig. S9), but to a lower extent than β-RA.

Glucose and lipid metabolism are under the control of metabolic hormones. Thus, HFHS diet induces hyperinsulinemia secondary to insulin resistance (Fig. 5M). In parallel, plasma glucagon levels are decreased and, consequently, the insulin/glucagon ratio is increased (Fig. 5N–O). Also, plasma levels of both gastric inhibitory polypeptide (GIP), a hormone that controls insulin secretion and promotes nutrient storage and inhibition of lipolysis in adipose tissue [20], and leptin, a hormone secreted by adipocytes that systemically controls fuel metabolism [3], increase under HFHS diet (Fig. 5P–Q). Importantly, β-RA treatment partially normalizes the serum levels of the metabolic hormones, consistent with the reduction of the content of WAT and the normalization of energy metabolism and insulin and leptin resistance (Fig. 5M–Q). Moreover, the metabolomic analysis in the serum of the DIO mice reveals an increase in the levels of the amino acids asparagine (ASN), glutamate (GLU), proline (PRO), serine (SER), homocysteine (HCY), s-adenosyl-homocysteine (SAH) and betaine (BT), which is characteristic of obesity and NALFD [21]. Also, the serum levels of leucine (LEU), valine (VAL) and tryptophan (TRP) decrease in DIO mice (Fig. 5R). Importantly, β-RA treatment normalizes the serum amino acids profile (Fig. 5R).

2.5. *The therapeutic effects of β-RA are also observed in mice that are already obese mice*

To test whether β-RA can also reduce the body weight and normalizes the levels of key metabolites in already obese mice, we treated DIO mice with β-RA for 7 weeks after 9 weeks under HFHS diet (HFHS16/BRA7) (Fig. 2A). β-RA reduces the body weight in HFHS16/BRA7 mice, with a more drastic effect in females than in males (Figs. 2B–C, S11A–B). However, the body weight reduction with β-RA is less intense than the body weight reduction observed with subcutaneous administration of semaglutide treatment (Fig. S10). Therefore, β-RA not only prevents the increase in body weight, but also reduces the body weight in already obese mice. Moreover, the reduced body weight in mice after β-RA treatment is mainly caused by the decrease in the content of WAT while still preserving the weight of skeletal muscle (Fig. S11C–F). These changes in body weight result in the normalization of plasma triglycerides and cholesterol, an improvement in glucose homeostasis characterized by the normalization of the insulin/glucagon ratio, as well as levels of GIP and leptin (Fig. S11G–S). Accordingly, after 7 weeks on the HFHS + β-RA diet, the livers of mice do not exhibit features of steatosis under hematoxylin & eosin (H&E) and oil-red (ORO) stains (Fig. S11T–Y); and the epididymal WAT does not show hypertrophic adipocytes (Fig. S11Z–AB). These effects are due, at least in part, to the normalization of the CoQ_9 levels in mitochondria of WAT, a mechanism that is not observed in either liver or skeletal muscle (Fig S11AC–AE).

Since β-RA acts in the mitochondrial CoQ biosynthetic pathway and considering that mitochondrial UCP1 is a redox-regulated protein able to burn fat through mitochondrial uncoupling, we also analyzed the expression of UCP1 in WAT. The levels of UCP1 do not significantly differ between animals fed with either standard or HFHS diets (Fig. S12A–F, M–R). Notably, β-RA therapy slightly increases the

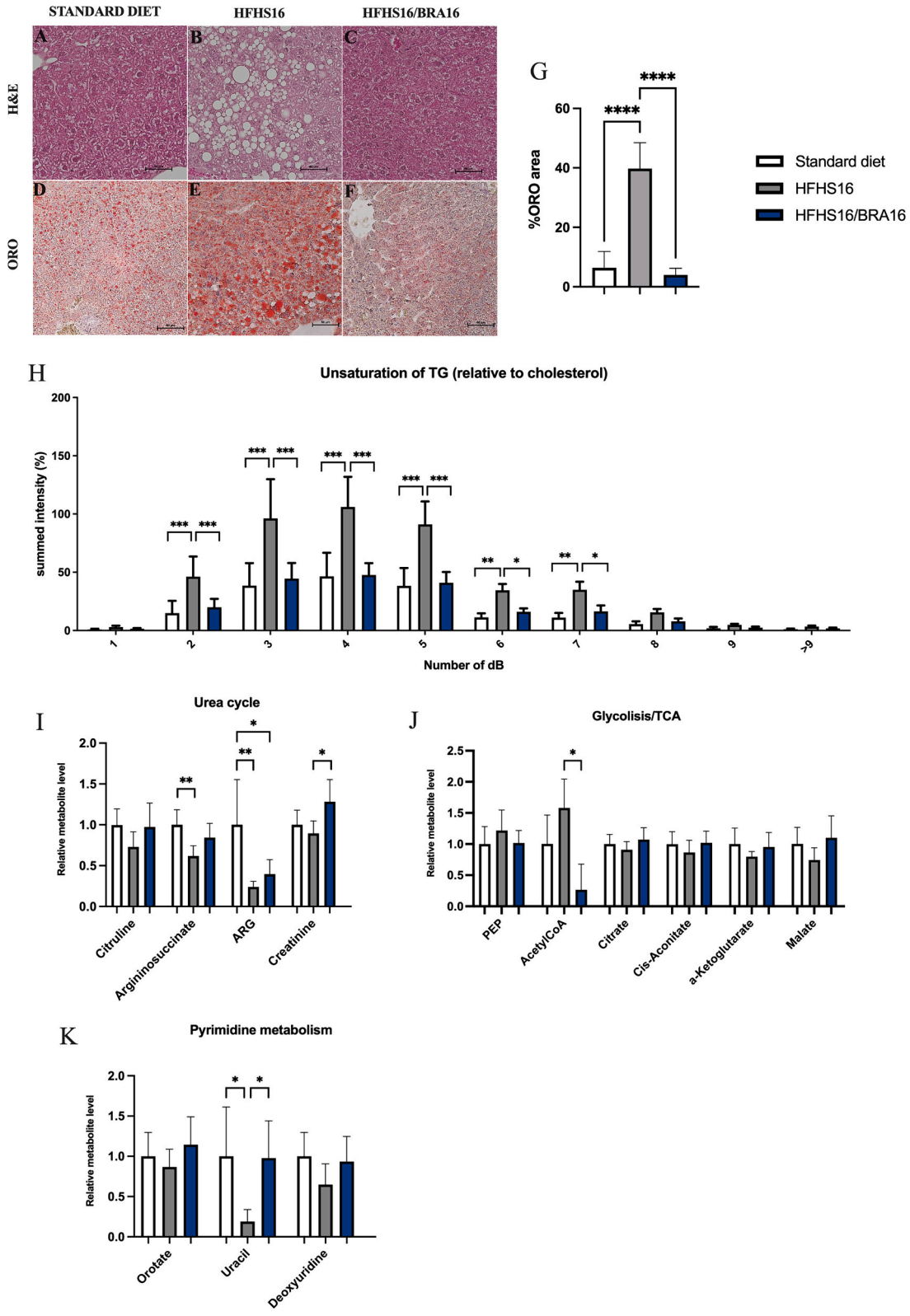

Fig. 3. Morphologic and metabolic characterization of the liver in DIO mice, and the effect β-RA treatment. (A–C) Representative H&E staining of paraffin sections from the liver. (D–F) Representative Oil red O (ORO) staining of OCT-embedded liver sections. (G) Quantification of ORO-positive stained area versus total liver area in OCT-embedded liver sections ($n = 10$ for control group, $n = 7$ for HFHS16 and n = 7 for HFHS16/BRA16). (H) Levels of triglycerides represented by their number of double bonds, relative to cholesterol levels, in the liver. (I–J) Hepatic levels of metabolites related to urea cycle (K), glycolysis/TCA cycle (L) and pyrimidine metabolism. (N–O). Data from liver of mice fed with either standard diet, HFHS diet or HFHS +0.33 % β-RA. Data are expressed as mean ± SD. * $p < 0.05$, ** $p < 0.01$, *** $p < 0.001$; significance was assessed by one-way ANOVA tests with Tukey's post hoc test multiple comparisons test. Each point represents a biological replicate $n = 5$ for control and HFHS group and $n = 6$ for HFHS16/BRA7 group.

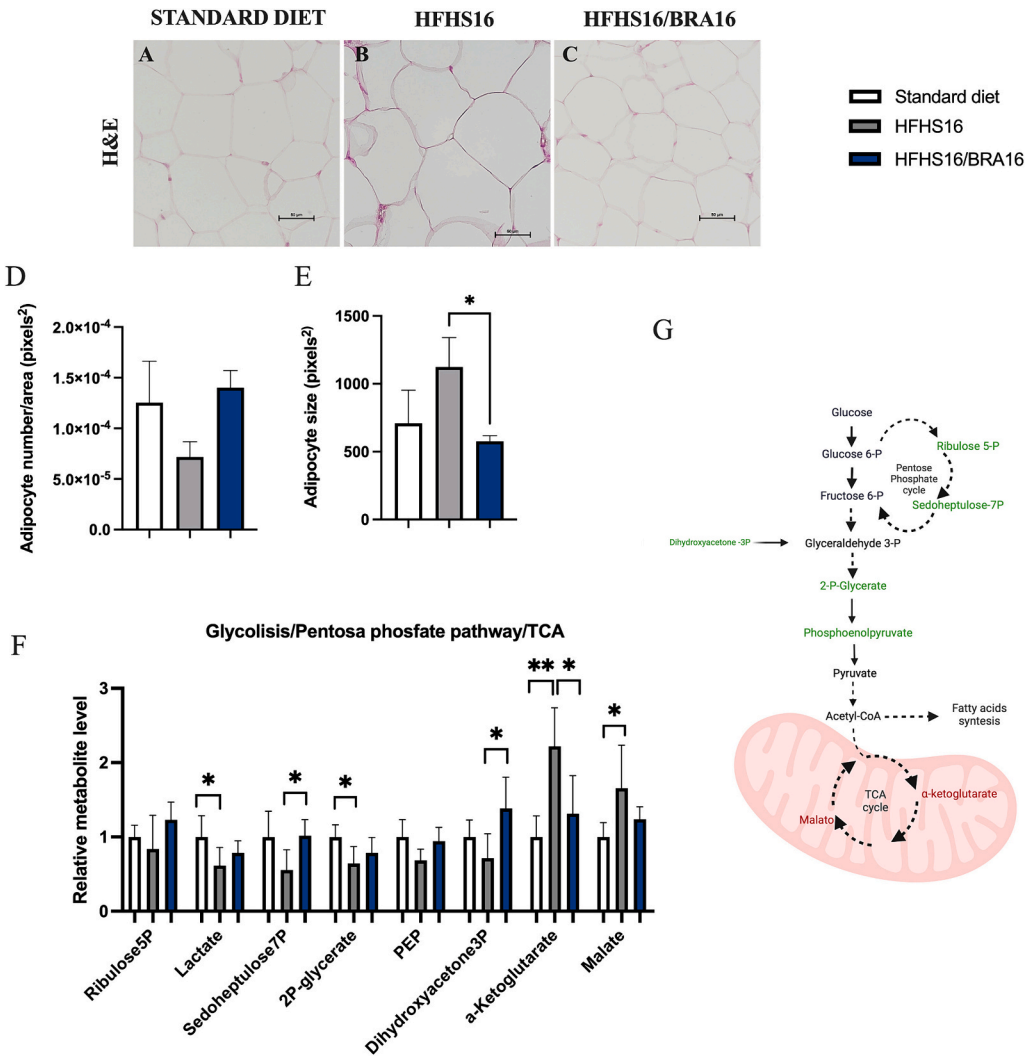

Fig. 4. Morphologic and metabolic characterization of the WAT in DIO mice, and the effect β-RA treatment. (A–C) Representative hematoxylin and eosin (H&E) staining of WAT paraffin sections. (D, E) Quantification of the number per area (D) and size (E) of the adipocytes ($n = 3$ for each group). (F) Key metabolites related to glycolysis, pentose phosphate pathway and TCA (n = 5 for control and HFHS group and n = 6 for HFHS16/BRA7 group). (K) Scheme of the involved metabolic pathway. Data from WAT of mice fed with either standard diet, HFHS diet or HFHS +0.33 % β-RA. Data are expressed as mean ± SD. * $p < 0.05$, ** $p < 0.01$. Significance was assessed by one-way ANOVA tests with Tukey's post hoc test multiple comparisons test.

expression of UCP1, in both males and females, independently of the regimen of administration, i.e., HFHS16/BRA16 or HFHS16/BRA7 (Fig. S12G–L, S–X). Interestingly, the effect of β-RA treatment was more pronounced in HFHS16/BRA7 mice (Fig. S12J–L, V–X) than in HFHS16/BRA16 mice (Fig. S12G–I, S–U), a fact that may be attributed to the weight loss that these mice are actively experiencing, through an adaption of the metabolism of the white adipocytes. These data slightly correlate with the UCP1 levels in brown adipose tissue (BAT) (Fig. S12Y and Z). These results suggest that β-RA treatment has an anti-obesity effect due, at least in part, to its mitochondrial actions.

Taken together, these data demonstrate that β-RA protects and rescues against diet-induced obesity and normalizes the levels of key metabolites, most likely due to the reduction of adiposity as a primary event.

2.6. *The ADME study supports the transitional potential of β-RA*

The current study and other independent preclinical studies have tested the administration of β-RA as a potential therapy for primary and secondary CoQ deficiencies [6–11]. However, there is no available data regarding the metabolic and pharmacokinetic properties of this compound. Using liver microsomes, we have identified β-RA as a compound with a long half-life and low clearance dependent on cytochrome P450 isoforms (Table 1), compared to verapamil, a high clearance compound. Importantly, the reduced cytochrome P450-dependent clearance is comparable in both mouse and human microsomes (Table 1).

Then, we determined the pharmacokinetics of β-RA by intravenous administration (50 mg/kg b.w.) in C57BL/6J mice. As shown in Fig. S13, the profile of time and plasma (Fig. S13A) and liver (Fig. S13B) concentration of β-RA indicates that β-RA has a two-phase elimination (before and after 60 min). The pharmacokinetic parameters of β-RA in mouse plasma indicate that its half-life is 197.98 min; the time of maximum observed concentration is 5 min; the maximum observed concentration is 1.63×10^5 ng/ml; and its area under the curve (AUC 0-t) is 3.5×10^6 ng/ml x min (Table 2). The volume distribution (Vz) of β-RA is 1.42×10^5 (mg/kg)/(ng/ml) and the clearance (Cl) is 5.47×10^5 (mg/kg)/(ng/ml) (Table 2). These data suggest that a sustained administration of β-RA is required to maintain therapeutically relevant concentrations of β-RA in plasma, supporting the experimental administration in the chow for long term in vivo studies.

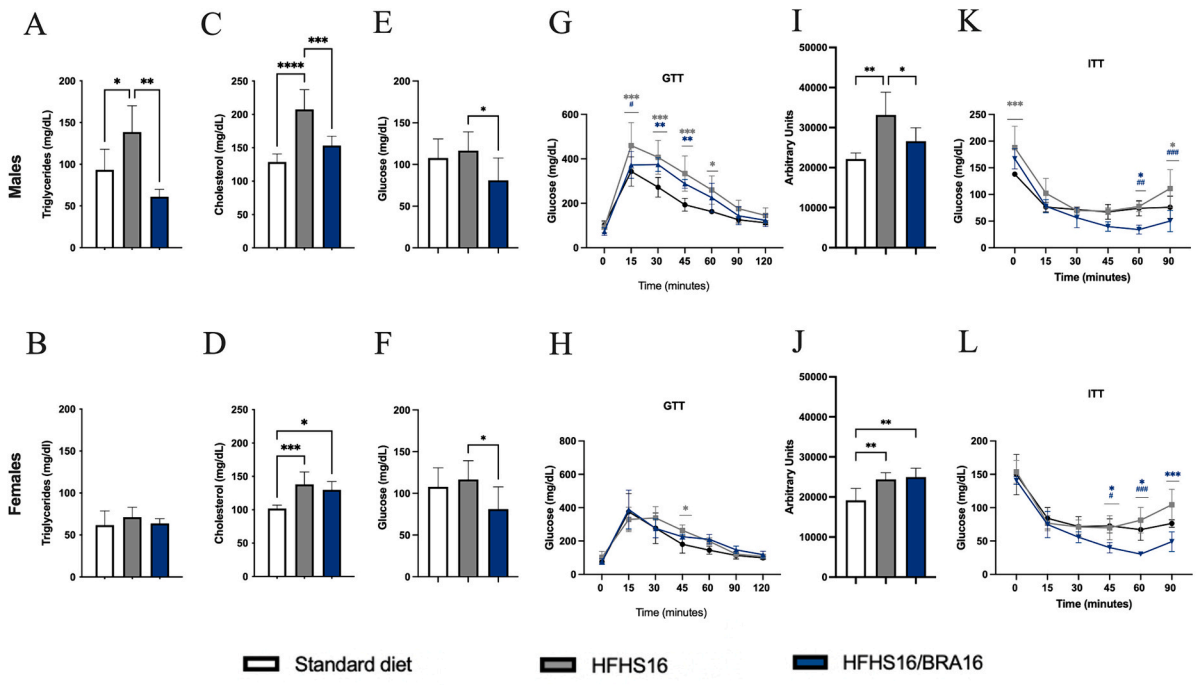

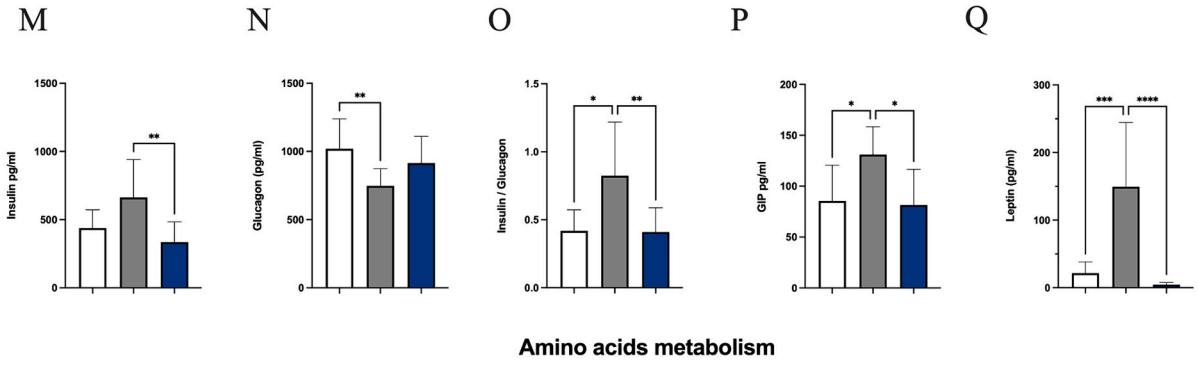

Amino acids metabolism

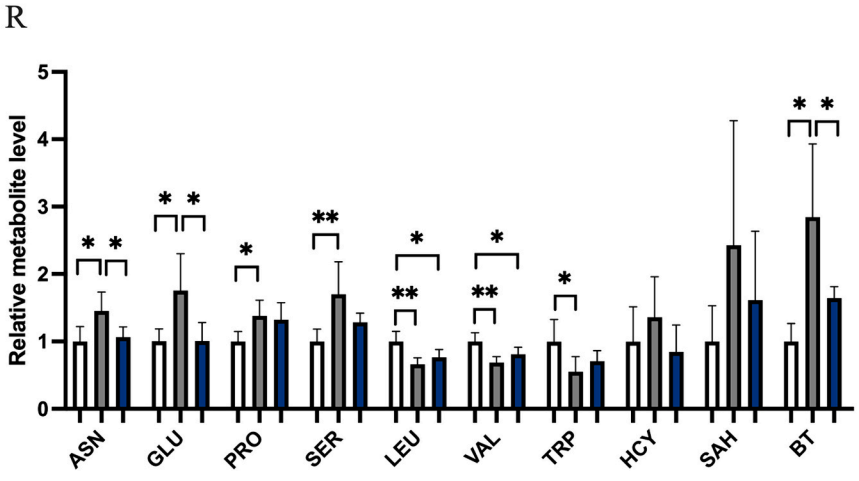

(caption on next page)

Fig. 5. Metabolic characterization of the serum of DIO mice, and the effect β-RA treatment. (A–F) Serum lipid and glucose profile, represented by levels of triglycerides (A, B) (n = 6 for control group and *n* = 4 for HFHS16 and HFHS16/BRA16 groups in male; n = 5 for control and HFHS16 group, and n = 4 for HFHS16/BRA16 group), cholesterol (C, D) (n = 6 for each group in males; n = 7 for control group, n = 6 for HFHS16 group and n = 4 for HFHS16/BRA16 group in female) and glucose (E, F) (*n* = 8 for each group in males and *n* = 11 for each group in females) in male (A, C, E) and female (B, C, F) mice. (G–H) Serum glucose levels following the glucose tolerance test (GTT) (n = 5 for each group in males and n = 6 for each group in females). (I–J) Area under the curve (AUC) from GTT in male (I) and female (J) mice (n = 5 for each group in males and n = 6 for each group in females). (K–L) Serum glucose levels following the insulin tolerance test (ITT) in male (K) and female (L) mice (n = 4 for control group, n = 5 for HFHS16 group and n = 4 for HFHS16/BRA16 group in males and females). (M–Q) Quantification of insulin levels (M) (n = 8 for each group), glucagon levels (N) (*n* = 13 for each group), insulin/glucagon ratio (O) (n = 8 for each group), GIP levels (P) (*n* = 9 for each group) and leptin levels (Q) (n = 8 for control and HFHS16/BRA16 groups, and n = 10 for HFHS16 group) in the mice serum. (R) Serum levels of metabolites related to amino acid metabolism in mice (n = 5 for control and HFHS group and n = 6 for HFHS16/BRA7 group). Data from serum of mice fed with either standard diet, HFHS diet or HFHS +0.33 % β-RA diet. Data are expressed as mean ± SD. * $p < 0.05$, ** $p < 0.01$, *** $p < 0.001$. Significance was assessed by one-way ANOVA tests with Tukey's post hoc test multiple comparisons test.

Table 1
Metabolic stability of β-RA, compared to a known compound, verapamil.

Compound	Mouse liver microsomes		Human liver microsomes	
	$T_{1/2}$ (min)	CL_{int} (ml/min/mg pt)	$T_{1/2}$ (min)	CL_{int} (ml/min/mg pt)
β-RA	>60	<11	>60	<51
Verapamil	3.02	221	1.98	1578

$T_{1/2}$ (min) = half-life; CL_{int} (ml/min/mg pt) = intrinsic clearance.

Table 2
Pharmacokinetic parameters of β-RA in mice.

Parameter	Units	Value
Lambda_z	1/min	0.0035
$T_{1/2}$	min	197.98
Tmax	min	5.00
Cmax	ng/ml	1.63×10^5
Clast/Cmax		9.81×10^5
AUC 0-t	ng/ml × min	3.50×10^6
AUC 0-inf	ng/ml × min	0.99
AUC 0-t/0-inf		1.62×10^8
AUMC	ng/ml × min^2	46.25
MRT	min	0.0040
Vz	(mg/kg)/(ng/ml)	1.42×10^5
Cl	(mg/kg)/(ng/ml)/min	5.47×10^5

Lambda_z = first order rate constant associated with the terminal (log-linear) portion of the curve. Estimated by linear regression of time vs. log concentration; $T_{1/2}$: half-life; Tmax = time of maximum observed concentration; Cmax = maximum observed concentration, occurring at Tmax; Cl = clearance; Clast = total body clearance for extravascular administration; AUC 0-t: area under the curve, from time 0 to time t; AUC 0-inf: area under the curve, from time 0 to the time that the drug is no longer present; AUMC 0-inf_obs = area under the first moment curve (AUMC), from time 0 to the time that the drug is no longer present; MRT: mean residence time; Vz = volume of distribution; Cl = Clearance.

3. Discussion

New therapeutic options for obesity and MASLD are challenging due to the difficulties of identifying novel and safe therapeutic mechanisms with translational potential. Here, we first confirm that hypertrophied white adipocytes in DIO mice harbor secondary CoQ deficiency. Then, we discover that β-RA, a natural phenolic compound used by the food industry as a taste enhancer, normalizes mitochondrial CoQ metabolism in WAT, which leads to a metabolic rewiring. Moreover, β-RA promotes a modification in the hepatic transcriptome that results in an induction of lipid catabolism. Those actions specifically prevent and reduce the accumulation of WAT in a preclinical model of diet-induced obesity. Consequently, β-RA also avoids the ectopic fat accumulation in the liver, thus preventing MASLD.

CoQ deficiency can be primarily caused by defects in the CoQ biosynthetic genes or secondarily to other conditions [22,23], including metabolic syndrome [5]. Animal models of primary CoQ deficiency have been very valuable to identify new functions of CoQ and pathomechanisms of CoQ deficiency and to evaluate potential therapies [15,24]. Among those therapies, β-RA has emerged as an effective therapy in different mouse models of primary CoQ deficiency with either encephalopathy or nephrotic syndrome [6–10]. In all cases, β-RA has been orally administered in the drinking water or the chow, and the compound is detectable in serum and tissues [7,8]. This mode of administration seems to be optimal since, although the compound is not metabolized by mouse or human microsomes, its half-life and other pharmacokinetic parameters suggest the need of a sustained administration to maintain optimal levels of the compound in serum and tissues. This is similar to the results of the pharmacokinetic analyses of other small phenolic compounds, including 3,4-dihydroxybenzoic acid (3,4-diHB) or protocatechuic acid [25,26].

Although β-RA therapy is promising in cases of primary CoQ deficiency, its potential application in cases of secondary CoQ deficiencies has not been evaluated yet. Here, we confirm that secondary CoQ deficiency is a common feature in mitochondria of WAT in animal models of obesity [5,14], a fact that has been also reported in humans with insulin resistance [5]. Importantly, we demonstrate that β-RA therapy can be also effective in secondary CoQ deficiencies, particularly in obesity and insulin resistance. β-RA supplementation normalizes CoQ_9 levels in mitochondria of WAT of DIO mice, most likely due to a stimulation in the expression of the COQ5 and COQ7 proteins, which are components of the Complex Q [24]. The normalization of the mitochondrial CoQ levels may contribute to the stimulation in the expression of UCP1, a thermogenic protein with fat-burning properties. The association of CoQ and UCP1 has been previously reported [27], although its role in a physiological context is still controversial [28–30]. Nevertheless, a recent study has shown that CoQ impacts mitochondrial respiration of brown and beige adipocytes through the modulation of UCP1 expression [31]. However, it cannot be discarded that β-RA directly impacts UCP1 in adipose tissue nor influences the whole mitochondrial metabolism. In any case, the normalization of the mitochondrial CoQ levels may contribute to a metabolic rewiring that normalizes the adipocytes phenotype.

The effect of β-RA in modulating mitochondrial CoQ metabolism and linked pathways may contribute to a profound reduction in the WAT content, resulting in a decrease in the animals' body weight and a prevention in the development of MASLD. The link between β-RA, mitochondrial CoQ metabolism and reduction in WAT content is reinforced by that fact that 4HB, a β-RA analog and natural precursor of CoQ biosynthesis, partially normalizes the mitochondrial CoQ_9 levels and reduces the WAT content and the animals' body weight. The differences observed among each compound can be partially attributed to their distinct actions within the CoQ biosynthetic pathway. For example, β-RA has the potential to bypass defects in COQ7 or COQ9 since it contains the hydroxyl group that is incorporated in the benzoquinone ring by the step catalyzed by COQ7-COQ9 [6,8]; VA could bypass defects in COQ6 since it contains the methyl group that is incorporated in the benzoquinone ring by the steps catalyzed by COQ6 and COQ3 [16]; and 4HB could enhance COQ2 activity through a substrate-enhancement therapeutic mechanism [12,32]. Another β-RA analog, 3,4-diHB, which could bypass COQ6 defects [16], has also been reported to attenuate diet-induced obesity [33]. However, 4HB and 3,4-diHB each individually

reduce the body weight by only 7–12 %, while β-RA reduces it by 29–33 %, a value that is still below of the anti-obesity effects observed by semaglutide in DIO mice [34].

Although the effect of β-RA on CoQ metabolism in WAT could partially explain the reduction in the WAT content, we also found that β-RA induces transcriptomics changes that modify lipid metabolism in the liver. Specifically, β-RA activates genes involved in fatty acids β oxidation and triacylglycerol degradation, while inhibits genes involved in cholesterol biosynthesis. Importantly, our analyses of the canonical pathways and upstream regulators predict that these effects could be mediated through the nuclear receptor LXR and the transcription factor HNF4α, both involved in the regulation of lipid metabolism in the liver [35]. In fact, mutations in HNF4α are associated to diabetes and metabolic disorders [18], and both LXR and HNF4α have been also proposed as therapeutic targets for obesity and MASLD [35,36]. Interestingly, a recent study has shown that N-trans-caffeoyltyramine acts as HNF4α agonist and, when orally administrated, leads to a prevention of weight gain and hepatic steatosis in mice fed with HFD [37]. N-trans-caffeoyltyramine is a hydroxycinnamic acid, which has the benzene ring hydroxylated, as β-RA and others hydroxybenzoic acids derivatives [38]. Therefore, we speculate that β-RA could act as HNF4α agonist, although that must be evaluated in future studies. The dual actions of β-RA on CoQ metabolism, coupled with the activation of LXR and HNF4α, induce metabolic functions that actively utilize fuel; however, it is crucial to evaluate energy expenditure in future studies. Nevertheless, this may explain the intense effect of β-RA in preventing body weight gain in animals fed a HFHS diet, resulting in lower body weight compared to animals fed a standard diet, even with opposite differences in energy intake. Similar observations have been noted in preclinical models with others anti-obesity drugs employing different mechanisms of action [34,39].

Another important observation is that β-RA is effective in reducing the content of WAT when administered concomitantly with the initiation of HFHS diet and when the animals have already undergone 9 weeks of the HFHS diet, indicating that β-RA can be effective in both preventing and treating overweight and obesity. Moreover, β-RA prevention and treatment of the overweight/obesity resulted in a gradual and reversible reduction in body weight, suggesting a lack of toxic effects. In fact, β-RA has been supplemented at the same dose throughout the whole life of the animals fed with standard diet with no toxic side effects and even an increase in lifespan [7].

While our study emphasizes significant anti-obesity effects in vivo in the DIO model, we recognize several considerations that merit attention: 1) Although the PK characteristics of β-RA analogs are expected to be similar [25], we have not conducted an ADME study for each compound. This oversight could partially account for differences observed in the outcomes associated with each compound; 2) the ADME study was conducted via intravenous administration, which might not fully capture certain aspects of absorption and metabolism that are relevant to oral administration, and to a specific DIO model; 3) the involvement of HNF4α in the anti-obesity effects of β-RA must be further characterized; and 4) the conversion of the mouse dosage to its human equivalent necessitates thorough consideration, factoring in various elements such as compound metabolism and variances in body surface area.

In conclusion, our study identifies CoQ metabolism as a pathological and therapeutic target in obesity and MASLD and provides a potentially translatable therapeutic tool, with complementary mechanisms of actions, for the prevention and treatment of overweight and obesity.

4. Methods

4.1. Animals and treatments

C57BL/6J mice were used for this study. Specific experiments were also developed in nicotinamide nucleotide transhydrogenase knockout (NNT^{KO}) C57BL/6J mice, which are more prone to the obese phenotype [13]. Therefore, by using these mice we aimed to explore if the anti-obesity effects of β-RA was also observed in mice with more intense obese phenotype. The animals were housed in the Animal Facility of the University of Granada under an SPF zone on a 12-hr light/dark cycle with unlimited access to water and food. No inclusion or exclusion criteria were used to assign animals in each experimental group. All data were included in the results.

Eight-week-old mice were fed ad libitum for a period of 16 weeks with a standard lab diet (SAFE® 150, which provides 21 %, 12.6 % and 66.4 % energy from proteins, lipids and carbohydrates, respectively; 3028 kcal/kg) (standard diet group) or with a high-fat high-sucrose diet (HFHS) (SAFE® U8954P Version 0027, 30 % Lard and 37 % Sucrose, which provides 14,5 %, 53,8 % and 31,7 % energy from proteins, fat and carbohydrate, respectively; 5068.6 kcal/kg) (HFHS16 group). The diets were stored at 4 °C and replenished in the animal cages twice a week. β-resorcylic acid (β-RA) (Merck Life Science S.L.U, Madrid, Spain), vanillic acid (VA), 4-hydroxybenzoic acid (4HB) or CoQ_{10} were administered to the mice in the HFHS diet at a concentration of 0.33 % (*w*/w), corresponding to 23.9 mmol β-RA, 21.4 mmol VA, 19.6 mmol 4HB or 3.8 mmol CoQ_{10} in each kilogram od chow (HFHS16/BRA16, HFHS16/VA16, HFHS16/4HB16, HFHS16/CoQ16 groups). This range of doses is able to increase the levels of the specific compounds in plasma and tissues [7,8,11,40]. All groups were assessed at the same time during experiments. β-RA at 0.33 % has been previously reported to reduce body weight in wild type mice [7].

Mice began receiving the assigned treatments at 8 weeks of age, except in the HFHS16/BRA7 group, in which the treatments with β-RA started at 9 weeks after the start of the HFHS diet. Mice were monitored for 16 weeks before conducting studies at the end-of-experiment dissection and posterior analyses. Control and treated groups were assessed at the same time during experiments. The analyses were performed at the age indicated for each case. Animals were randomly assigned to experimental groups and mice from different cages were used to negate cage-specific effects. Data were randomly collected and processed.

Food intake was recorded experiment every three days for two weeks. Mice were housed in groups of 2–4 animals per cage. The body weights were recorded once a week. Mice were sacrificed at 6 months of age and the skeletal muscles (*gastrocnemius* and *vastus lateralis*), white adipose tissues (epididymal and inguinal) and the liver were dissected and weighed on a laboratory scale.

For analytical experiments, only *gastrocnemius* and epididymal WAT were used to evaluate the involvement of skeletal muscle and WAT.

To compare the effects of β-RA with those of semaglutide, a highly effective anti-obesity drug, mice were fed a HFHS diet for 11 weeks. At week 9, either β-RA was introduced into the diet at a concentration of 0.33 % (*w*/w) (HFHS11/BRA2) or semaglutide was subcutaneously injected at a dose of 10 nmol/kg b.w., dissolved in phosphate-buffered saline, twice daily (HFHS11/Segmaglu2) [34].

4.2. LC–MS/MS analysis of β-RA

Mice were treated with an intraperitoneal (i.v.) injection of β-RA at a dose of 50 mg/kg b.w, and mice were sacrificed at 5, 15, 30, 60, 240, 480, 720, 960 and 1440 min after the injection. Blood samples were extracted and centrifuged to obtain the plasma. The mouse plasma and tissue liver samples were thawed by leaving them at room temperature. A 50.0 μl aliquot of each mouse plasma sample was mixed with 150.0 μl of cold AcN containing the internal standard (200 ng/ml). After vortex mixing for 1 min, the samples were centrifuged at 13300 rpm for 15 min at 4 °C. Following centrifugation, a 150 μl aliquot of the supernatant was transferred to an autosampler vial for LCMS analysis. As for the liver tissue samples, they were homogenized with a 3.5 volume of phosphate buffer saline (PBS) using the MACS Dissociator (Miltenyi Biotec), a benchtop instrument for the automated dissociation of tissues. Then, a 50 μl volume of the homogenate was combined with 150 μl of ice-cold

methanol containing the internal standard (final concentration 148.5 ng/ml). The mixture was vortexed for 1 min and then subjected to centrifugation at 13300 rpm for 15 min at 4 °C. Subsequently, an aliquot of 160 μl of the resulting supernatant was transferred to a vial for LCMS analysis.

The supernatants were analyzed using an Agilent 1290 Infinity coupled to API4000 AB Sciex MS detector with an electrospray ionization in negative mode. The analytical separation column was a Atlantis T3, 3 μm, 2.1 × 50 mm column (Waters, Spain) and the flow rate was 0.4 ml/min. The mobile phase consisted of two solutions: eluent A (0.1 % formic acid in 10 % acetonitrile) and eluent B (0.1 % formic acid in 90 % acetonitrile). Samples were eluted over 5 min with a gradient as follows: 0–0.5 min, 5 % eluent B; 0.5–2.70 min, 95 % eluent B; 2.70–4.00 min, 95 % eluent B; 4.00–4.10 min, 5 % eluent B; 4.10–5 min, 5 % eluent B. Source temperatures was set at 400 °C. Nitrogen was used as curtain gas (20 psi), nebulizer gas (60 psi), desolvation gas (45 psi) and as collision gas (4 psi). Mass spectrometry analyses were carried out in multiple reaction monitoring mode (MRM) at the following transitions: *m/z* 152.899/65.0for β-RA and 137.106/64.893 for the internal standard (salicylic acid).

Quantification of β-RA levels in treated mouse plasma samples was achieved according to a previously validated method. Briefly, blank mouse plasma samples were spiked with standard solutions of β-RA (50–6500 ng/ml) and an internal standard (200 ng/ml). Analyte extraction was performed using ice-cold acetonitrile. Recovery values ranged from 54 % to 66 % depending on the concentration. Method linearity was established with a regression coefficient (r) of 0.9996.

Additionally, the back-calculated standards provided a maximum variation of 5.53 % (CV%) and the accuracy ranged between 87.3 % and 108 %, referring to the nominal concentration value. Similarly, mouse liver tissue samples were quantified according to a previously validated method. Briefly, mouse liver tissue samples were homogenized with a 3.5 volume of PBS. Then, 50 μl of liver homogenate was extracted with 150 μl of ice-cold methanol. Method recovery ranged from 108 % to 130 % depending on the concentrations. Calibration standard curves were established from 8 to 1024 ng/ml, and method linearity was set at $r = 0.9993$.

4.3. Histology and immunohistochemistry

Tissues were fixed in formalin (24 h), processed and embedded in paraffin. Multiple sections (4 μm thickness) were deparaffinized with xylene and stained with hematoxylin and eosin (H&E) (Merck Life Science S.L.U, Madrid, Spain). Immunohistochemistry was carried out on the same sections using the following primary antibody UCP1 (U6382, Sigma-Aldrich) at 1:500 dilution. The Dako Animal Research Kit for mouse primary antibodies (Dako, Agilent Technologies, Madrid, Spain) was used for the qualitative identification of antigens by fluorescence microscopy. Alternatively, liver tissue samples were included in OCT (Tissue-Teck). Sections (8 μm) were stained with Oil Red (Merck Life Science S.L.U, Madrid, Spain) for lipid staining. Sections were examined at 40–400 magnifications with a Nikon Eclipse Ni—U microscope (Werfen, Madrid, Spain), and the images were scanned under equal light conditions with the NIS-Elements Br computer software (Werfen, Madrid, Spain). For lipid content quantification, liver slides were analyzed with ImageJ software (NH, Bethesda, USA) as ORO-positive area versus the total area.

4.4. Plasma analysis

Blood samples were obtained from submandibular vein puncture and collected in K_3-ethylenediaminetetraacetic acid (EDTA) tubes (Kima, VWR, Barcelona, Spain). The plasma was extracted from the blood sample via centrifugation at 4500 *g* for 10 min at 4 °C and then frozen at −80 °C. Biochemical analyses were carried out in a biochemical analyzer Bs-200 (Shenzhen Mindray Bio-Medical Electronics Co., Ltd., Shenzhen, China) using reagents from Spinreact.

Insulin concentration was assessed using the Mouse INS ELISA Kit (EM0260) following the manufacturer's instructions (FineTest, Labclinics, Barcelona, Spain). The results were expressed in picograms per milliliter. Glucagon concentration was quantified using the Mouse GC ELISA Kit (EM0562) according to the manufacturer's instructions (FineTest, Labclinics, Barcelona, Spain). The results were expressed in picograms per milliliter. GIP concentration was measured using the Mouse GIP ELISA Kit (EM0277) according to the manufacturer's instructions (FineTest, Labclinics, Barcelona, Spain). The results were expressed in picograms per milliliter. Leptin concentration was quantified using the Mouse LEP ELISa Kit (RAB0334) according to the manufacturer's instructions (Millipore, Saint Louis, USA). The results were expressed in picograms per milliliter.

4.5. In vivo metabolic assays

For glucose-tolerance tests (GTTs) and insulin tolerance tests (ITTS), mice were fasted for 18 h or 4 h, respectively, with free access to water. For GTTs, the mice received a 50 % glucose solution in water at a dose of 2 g/kg body weight by i.p. injection. For ITTs, the mice received insulin injections of 0.75 U kg^{-1} by i.p. injection. Mice were bled from a tail clip and blood glucose was measured with a handheld glucometer before glucose administration (time 0) and 15, 30, 45, 60, 90, and 120 min after.

4.6. Sample preparation and western blot analyses in tissues

For sample preparation, a glass Teflon homogenizer was used to homogenize the mouse WAT, liver, skeletal muscle and brown adipose tissue samples at 1100 rpm in a T-PER® buffer (Thermo Scientific, Madrid, Spain) with protease inhibitor cocktail (Pierce). Homogenates were sonicated and centrifuged at 1000 ×*g* for 5 min at 4 °C, and the resultant supernatants were used for the Western blot analysis. About 40 μg of protein from the sample extracts were electrophoresed in 12 % Mini-PROTEAN TGXTM prescast gels (Bio-Rad) using the electrophoresis system mini-PROTEAN Tetra Cell (Bio-Rad). Proteins were transferred onto PVDF 0.45 μm membranes using a Trans-Blot Cell (Bio-Rad) and probed with target antibodies. Protein-antibody interactions were detected using peroxidase conjugated horse anti-mouse, anti-rabbit, or anti-goat IgG antibodies and Amersham ECLTM Prime Western Blotting Detection Reagent (GE Healthcare, Buckinghamshire, UK). Band quantification was carried out using a ChemiDoc MP Imaging System (Bio-Rad) and ImageJ software (NH, Bethesda, USA). Protein band intensity was normalized to VDAC1 for mitochondrial proteins. The data were expressed in terms of percent relative to wild-type mice.

The following primary antibodies were used: anti-COQ5 (17453-AP, Proteintech, Manchester, UK), anti-COQ7 (Proteintech, 15083-1-AP), anti-CABC1 (H00056997M-04A, Abnova), anti-COQ9 (PA5-24816, Invitrogen), anti-UCP1 (U6382, Sigma-Aldrich), anti-VDAC (ab14734, Abcam).

The same samples from mice in the standard diet and in HFHS diet were used in the evaluation of the effects of β-RA and the effects of other compounds (VA, 4HB and CoQ_{10}.

4.7. Transcriptome analysis by RNA-Seq

The RNeasy Lipid Tissue Mini Kit (Qiagen) was used to extract total RNAs from the liver and WAT, while RNA from skeletal muscle was extracted using Trizol (Invitrogen). Seven animals (three females and four males) were included in each experimental group. The RNAs were precipitated, and their quality and quantity assessed using an Agilent Bioanalyzer 2100 and an RNA 6000 chip (Agilent Technologies). The cDNA libraries were then constructed using the TruSeq RNA Sample Prep Kit v2 (Illumina, Inc.) and their quality checked using an Agilent Bioanalyzer 2100 and a DNA 1000 chip (Agilent Technologies). The

libraries were Paired End sequenced in a HiSeq 4000 system (Illumina, Inc.) at Macrogen Inc. We aimed for 4–5 Giga Bases outcome per sample. The quality of the resulting sequencing reads was assessed using FastQC. The GRCm39 fasta and gtf files of the reference mouse genome were downloaded from the Ensembl database and indexed using the bwtsw option of BWA. BWA, combined with xa2multi.pl and SAMtools, was also used for aligning the sequencing reads against the reference genome, and HTSeq was used for counting the number of reads aligned to each genomic locus. The alignments and counting were carried out in our local server following the protocols as described [41].

After elimination of the genomic loci that aligned to at least a read in at least 2 samples and normalization of the read counts by library size, the differential gene expression was detected [11], using the Generalized Linear Model (glmLRT option) statistic in EdgeR [42]. We used a 0.05 *P*-level threshold after False Discovery Rate correction for type I error. Annotation of the differentially expressed genes was obtained from the Mouse Genome Informatics (http://www.informatics.jax.org/). The transcripts that filled the inclusion criteria were then subjected to gene classification, using a databank based on hand-curated literature. The general canonical pathways and upstream regulators implicated for the significantly changed transcripts were generated by Ingenuity Pathway Analysis (IPA; Ingenuity Systems, Redwood City, CA, USA) before being evaluated and *P*-values <0.01 were considered significant. z-Score indicates a predicted activation or inhibition of a pathway/gene, where a negative z value connotes an overall pathway's inhibition (represented in blue), and a positive z value connotes an overall pathway's activation (represented in orange). The prediction is based on the gene expression profile, using the IPA software algorithms that front the data with the existing literature. Ingenuity Pathway Analysis (IPA; Ingenuity Systems, Redwood City, CA, USA) was also used for generating the gene expression heatmaps.

4.8. Liquid chromatography – mass spectrometry (LC-MS) – based metabolomics

For metabolite extraction, 10 μl of serum was diluted in 1 ml of a lysis buffer composed of methanol/acetonitrile/H_2O (2:2:1) and shook for 10 min at 4 °C before centrifugation for 15 min at full speed and 4 °C. For WAT, SKM and liver samples, 35–50 mg of tissue was ground in a mortar under liquid nitrogen, and metabolites were extracted by adding 500 μl lysis buffer and shaking for 20 min before centrifugation. The supernatants were collected and used for LC-MS analysis. The LC-MS analysis procedure and parameters were as described before [11]. LC-MS analysis was performed on an Exactive mass spectrometer (Thermo Scientific) coupled with a Dionex Ultimate 3000 autosampler and pump (Thermo Scientific). The MS operated in polarity-switching mode with spray voltages of 4.5 kV and – 3.5 kV. Metabolites were separated using a Sequant ZIC-pHILIC column (2.1 × 150 mm, 5 μm, guard column 2.1 × 20 mm, 5 μm; Merck) with elution buffers acetonitrile and eluent A (20 mM $(NH_4)_2CO_3$, 0.1 % NH_4OH in ULC/MS grade water (Biosolve). The flow rate was set at 150 μl/min and the gradient ranged from 20 % A to 60 % A in 20 min, followed by a wash at 80 % and re-equilibration at 20 % A. Metabolites were identified and quantified using TraceFinder software (Thermo Scientific). Metabolites were identified based on exact mass within 5 ppm and further validated by concordance with retention times of standards. The peak areas of the identified metabolites were in their respective linear range of detection. Peak intensities were normalized based on the total peak intensity of the total metabolites in order to correct for technical variations during mass spectrometry analysis [11].

4.9. Liquid chromatography – mass spectrometry (LC-MS) – based lipidomics

Lipids were extracted according to the method described by Bligh and Dyer [43]. Lipid extracts were dried under N_2 and then dissolved in 100 μl chloroform/methanol (1:1) and injected (10 μl) into a hydrophilic interaction liquid chromatography column (2.6 μm HILIC 100 Å, 50 × 4.6 mm, Phenomenex, CA). Lipid classes were separated by gradient elution on an Infinity II 1290 UPLC (Agilent, CA) at a flow rate of 1 ml/min. A mixture of acetonitrile and acetone (9/1; *v*/v) was used as solvent A, while solvent B consisted of a mixture of acetonitrile, H_2O (7/3; v/v) with 50 mM ammonium formate. Both solvents A and B contained 0.1 % formic acid (*v*/v). Gradient elution was performed as follows (time in min, %B): (0,0), (1, 50), (3, 50), (3.1, 100), (4, 100). Between successive samples, the column was not re-equilibrated. The column outflow was connected to a heated electrospray ionizationsource (hESI) of an Orbitrap Fusion mass spectrometer (Thermo Scientific, MA) operating at −3600 V in negative ionizationmode. The evaporator and ion transfer tube were set at 275 °C and 380 °C, respectively. Full scan measurements (MS1) in the mass range of 450 to 1150 amu were collected with a resolution of 120,000. Parallel data-dependent MS2 experiments were performed with HCD fragmentation set at 30 V, using the two-stage linear ion trap to generate up to 30 spectra per second.

The dried neutral lipids were dissolved in a mixture of chloroform and methanol (1/1; v/v). The lipids were separated on a Halo C18 fused core column (3.0 × 150 mm, 2.7 μm; Advanced Materials Tech, Wilmington, DE) with a gradient from 100 % methanol/water (1/1; v/v) to 100 % methanol/2-propanol (8/2; v/v) in 2 min and an additional 5.5 min elution with methanol/2-propanol. The elution took place at 40 °C and a flow rate of 600 μl/min. The column outflow was connected to an atmospheric pressure chemical ionization (APCI) source coupled to a Q Exactive HF mass spectrometer. Full scan measurements (MS1) in the mass range of 200 to 1100 amu were collected with a resolution of 120,000. Data processing using R-script was based on the 'XCMS' package for peak recognition and integration [44]. Lipid classes were identified based on retention time and molecular species were then compared with a lipid database generated in silico, with a mass accuracy of <0.003 Da.

4.10. Quantification of CoQ_9 and CoQ_{10} levels in mice tissues

After lipid extraction from the homogenized tissues, CoQ_9 and CoQ_{10} levels were determined via reversed-phase HPLC coupled to electrochemical detection, as previously described [45]. Then, a standard curve of CoQ_9 was used for a quantitative estimation. The results were expressed in nanograms of CoQ per milligram of protein.

4.11. Statistical analysis

The number of animals in each group were calculated in order to detect gross ~60 % changes in the biomarker measurements (based upon alpha = 0.05 and power of beta = 0.8). We used the application available at http://www.biomath.info/power/index.html Animals were randomly assigned to experimental groups in separate cages by the technician of the animal facility. Most statistical analyses were performed using the Prism 9 scientific software. In the figures, each point represents a biological replicate and data are expressed as the mean ± SD. A one-way or two-way ANOVA was used to compare the differences between experimental groups appropriate. Post hoc correction for multiple comparisons was carried out using Tukey's or Sidak's tests as appropriate. Studies with two experimental groups were evaluated using unpaired Student *t*-test. A *p*-value of <0.05 was considered to indicate statistical significance.

Funding

This work was supported by grants from the MCIN/AEI/10.13039/501100011033, Spain, and the ERDF (RTI2018-093503-B-100 and PID2021-126788OB-I00); and the Junta de Andalucía (grant numbers P20_00134 and PEER-0083-2020). S. L.-H. and P.G.-G. were supported by the 'FPU program' from the Ministerio de Universidades, Spain. A.H.-

G. and P.G.-G. were supported by the 'Plan Propio de Investigación' from the University of Granada. E.B.-C., L.J.-S. and J.C.-S. were supported by the Consejería de Salud, Junta de Andalucía, Spain. The authors also thank the support of the Unit of Excellence 'UNETE' from the University of Granada (reference UCE-PP2017-05).

Ethics approval and consent to participate

All animal manipulations and experiments were performed according to a protocol approved by the Institutional Animal Care and Use Committee of the University of Granada (procedure number 20/09/2021/136) and were in accordance with the European Convention for the Protection of Vertebrate Animals used for Experimental and Other Scientific Purposes (CETS#123) and with the Spanish law (R.D. 53/2013).

Consent for publication

All authors agree to the publication of this study.

CRediT authorship contribution statement

María Elena Díaz-Casado: Writing – review & editing, Writing – original draft, Visualization, Validation, Methodology, Investigation, Formal analysis, Data curation. **Pilar González-García:** Writing – review & editing, Visualization, Methodology, Investigation, Formal analysis, Data curation. **Sergio López-Herrador:** Writing – review & editing, Methodology, Investigation, Formal analysis. **Agustín Hidalgo-Gutiérrez:** Writing – review & editing, Methodology, Investigation, Formal analysis. **Laura Jiménez-Sánchez:** Writing – review & editing, Methodology, Investigation, Formal analysis. **Eliana Barriocanal-Casado:** Writing – review & editing, Investigation. **Mohammed Bakkali:** Writing – review & editing, Methodology, Investigation, Formal analysis. **Chris H.A. van de Lest:** Writing – review & editing, Methodology, Investigation. **Julia Corral-Sarasa:** Writing – review & editing, Methodology, Investigation. **Esther A. Zaal:** Writing – review & editing, Methodology, Investigation, Data curation. **Celia R. Berkers:** Writing – review & editing, Methodology, Investigation, Formal analysis. **Luis C. López:** Writing – review & editing, Writing – original draft, Supervision, Investigation, Funding acquisition, Formal analysis, Conceptualization.

Declaration of competing interest

The authors declare the following financial interests/personal relationships which may be considered as potential competing interests: Luis C. Lopez reports article publishing charges was provided by University of Granada. Luis C. Lopez has patent #WO2022123103 issued to No. If there are other authors, they declare that they have no known competing financial interests or personal relationships that could have appeared to influence the work reported in this paper.

Data availability

RNA-Seq data were generated as described above. The files have been uploaded to the repository Gene Expression Omnibus. The accession number is PRJNA1056451. All data can be found at https://www.ncbi.nlm.nih.gov/sra/PRJNA1056451.

Acknowledgements

We thank Seth Joel Drey for the English editing. We are grateful to Julio Ruiz (Universidad de Granada), José Pérez (Fundación Medina) and Jeroen Jansen (Utrecht University) for their technical support. We express our sincere gratitude to Prof. Sven Enerbäck for his invaluable scientific insights and thoughtful discussions throughout the course of this study. Some results shown in this article will constitute a section of the S.L.-H. doctoral thesis at the University of Granada.

Appendix A. Supplementary data

Supplementary data to this article can be found online at https://doi.org/10.1016/j.bbadis.2024.167283.

References

[1] D.J. Drucker, Diabetes, obesity, metabolism, and SARS-CoV-2 infection: the end of the beginning, Cell Metab. 33 (3) (2021) 479–498.
[2] D.H. Bessesen, L.F. Van Gaal, Progress and challenges in anti-obesity pharmacotherapy, Lancet Diabetes Endocrinol. 6 (3) (2018) 237–248.
[3] G. Valsamakis, P. Konstantakou, G. Mastorakos, New targets for drug treatment of obesity, Annu. Rev. Pharmacol. Toxicol. 57 (2017) 585–605.
[4] M. Qatanani, M.A. Lazar, Mechanisms of obesity-associated insulin resistance: many choices on the menu, Genes Dev. 21 (12) (2007) 1443–1455.
[5] D.J. Fazakerley, R. Chaudhuri, P. Yang, G.J. Maghzal, K.C. Thomas, J.R. Krycer, S. J. Humphrey, B.L. Parker, K.H. Fisher-Wellman, C.C. Meoli, N.J. Hoffman, C. Diskin, J.G. Burchfield, M.J. Cowley, W. Kaplan, Z. Modrusan, G. Kolumam, J. Y. Yang, D.L. Chen, D. Samocha-Bonet, J.R. Greenfield, K.L. Hoehn, R. Stocker, D. E. James, Mitochondrial CoQ deficiency is a common driver of mitochondrial oxidants and insulin resistance, Elife 7 (2018).
[6] Y. Wang, D. Oxer, S. Hekimi, Mitochondrial function and lifespan of mice with controlled ubiquinone biosynthesis, Nat. Commun. 6 (2015) 6393.
[7] A. Hidalgo-Gutierrez, E. Barriocanal-Casado, M.E. Diaz-Casado, P. Gonzalez-Garcia, R. Zenezini Chiozzi, D. Acuna-Castroviejo, L.C., Lopez, beta-RA targets mitochondrial metabolism and Adipogenesis, leading to therapeutic benefits against CoQ deficiency and age-related overweight, Biomedicines 9 (10) (2021).
[8] A. Hidalgo-Gutierrez, E. Barriocanal-Casado, M. Bakkali, M.E. Diaz-Casado, L. Sanchez-Maldonado, M. Romero, R.K. Sayed, C. Prehn, G. Escames, J. Duarte, D. Acuna-Castroviejo, L.C. Lopez, beta-RA reduces DMQ/CoQ ratio and rescues the encephalopathic phenotype in Coq9(R239X) mice, EMBO Mol. Med. 11 (1) (2019) 18.
[9] E. Widmeier, M. Airik, H. Hugo, D. Schapiro, J. Wedel, C.C. Ghosh, M. Nakayama, R. Schneider, A.M. Awad, A. Nag, J. Cho, M. Schueler, C.F. Clarke, R. Airik, F. Hildebrandt, Treatment with 2,4-Dihydroxybenzoic Acid Prevents FSGS Progression and Renal Fibrosis in Podocyte-Specific Coq6 Knockout Mice, J. Am. Soc, Nephrol, 2019.
[10] E. Widmeier, S. Yu, A. Nag, Y.W. Chung, M. Nakayama, L. Fernandez-Del-Rio, H. Hugo, D. Schapiro, F. Buerger, W.I. Choi, M. Helmstadter, J.W. Kim, J.H. Ryu, M.G. Lee, C.F. Clarke, F. Hildebrandt, H.Y. Gee, ADCK4 deficiency destabilizes the coenzyme Q complex, which is rescued by 2,4-Dihydroxybenzoic acid treatment, J. Am. Soc. Nephrol. 31 (6) (2020) 1191–1211.
[11] P. Gonzalez-Garcia, M.E. Diaz-Casado, A. Hidalgo-Gutierrez, L. Jimenez-Sanchez, M. Bakkali, E. Barriocanal-Casado, G. Escames, R.Z. Chiozzi, F. Vollmy, E.A. Zaal, C.R. Berkers, A.J.R. Heck, L.C. Lopez, The Q-junction and the inflammatory response are critical pathological and therapeutic factors in CoQ deficiency, Redox Biol. 55 (2022) 102403.
[12] J. Corral-Sarasa, J.M. Martinez-Galvez, P. Gonzalez-Garcia, O. Wendling, L. Jimenez-Sanchez, S. Lopez-Herrador, C.M. Quinzii, M.E. Diaz-Casado, L. C. Lopez, 4-Hydroxybenzoic acid rescues multisystemic disease and perinatal lethality in a mouse model of mitochondrial disease, Cell Rep. 43 (5) (2024) 114148.
[13] C.D.C. Navarro, T.R. Figueira, A. Francisco, G.A. Dal'Bo, J.A. Ronchi, J.C. Rovani, C.A.F. Escanhoela, H.C.F. Oliveira, R.F. Castilho, A.E. Vercesi, Redox imbalance due to the loss of mitochondrial NAD(P)-transhydrogenase markedly aggravates high fat diet-induced fatty liver disease in mice, Free Radic. Biol. Med. 113 (2017) 190–202.
[14] S. Bour, M.C. Carmona, A. Galinier, S. Caspar-Bauguil, L. Van Gaal, B. Staels, L. Penicaud, L. Casteilla, Coenzyme Q as an antiadipogenic factor, Antioxid. Redox Signal. 14 (3) (2011) 403–413.
[15] P. Gonzalez-Garcia, E. Barriocanal-Casado, M.E. Diaz-Casado, S. Lopez-Herrador, A. Hidalgo-Gutierrez, L.C. Lopez, Animal models of coenzyme Q deficiency: mechanistic and translational learnings, Antioxidants (Basel) 10 (11) (2021).
[16] M. Doimo, E. Trevisson, R. Airik, M. Bergdoll, C. Santos-Ocana, F. Hildebrandt, P. Navas, F. Pierrel, L. Salviati, Effect of vanillic acid on COQ6 mutants identified in patients with coenzyme Q deficiency, Biochim. Biophys. Acta 1842 (1) (2014) 1–6.
[17] M. Ozeir, U. Muhlenhoff, H. Webert, R. Lill, M. Fontecave, F. Pierrel, Coenzyme Q biosynthesis: Coq6 is required for the C5-hydroxylation reaction and substrate analogs rescue Coq6 deficiency, Chem. Biol. 18 (9) (2011) 1134–1142.
[18] F. Rastinejad, The protein architecture and allosteric landscape of HNF4alpha, Front Endocrinol (Lausanne) 14 (2023) 1219092.
[19] T.D. Cummins, C.R. Holden, B.E. Sansbury, A.A. Gibb, J. Shah, N. Zafar, Y. Tang, J. Hellmann, S.N. Rai, M. Spite, A. Bhatnagar, B.G. Hill, Metabolic remodeling of white adipose tissue in obesity, Am. J. Physiol. Endocrinol. Metab. 307 (3) (2014) E262–E277.
[20] J. Goralska, U. Razny, A. Polus, A. Dziewonska, A. Gruca, A. Zdzienicka, A. Dembinska-Kiec, B. Solnica, A. Micek, M. Kapusta, K. Slowinska-Solnica, M. Malczewska-Malec, Enhanced GIP secretion in obesity is associated with biochemical alteration and miRNA contribution to the development of liver steatosis, Nutrients 12 (2) (2020).

[21] O. Rom, Y. Liu, Z. Liu, Y. Zhao, J. Wu, A. Ghrayeb, L. Villacorta, Y. Fan, L. Chang, L. Wang, C. Liu, D. Yang, J. Song, J.C. Rech, Y. Guo, H. Wang, G. Zhao, W. Liang, Y. Koike, H. Lu, T. Koike, T. Hayek, S. Pennathur, C. Xi, B. Wen, D. Sun, M. T. Garcia-Barrio, M. Aviram, E. Gottlieb, I. Mor, W. Liu, J. Zhang, Y.E. Chen, Glycine-based treatment ameliorates NAFLD by modulating fatty acid oxidation, glutathione synthesis, and the gut microbiome, Sci. Transl. Med. 12 (572) (2020).
[22] M. Alcazar-Fabra, F. Rodriguez-Sanchez, E. Trevisson, G. Brea-Calvo, Primary coenzyme Q deficiencies: a literature review and online platform of clinical features to uncover genotype-phenotype correlations, Free Radic. Biol. Med. 167 (2021) 141–180.
[23] P. Navas, M.V. Cascajo, M. Alcazar-Fabra, J.D. Hernandez-Camacho, A. Sanchez-Cuesta, A.B.C. Rodriguez, M. Ballesteros-Simarro, A. Arroyo-Luque, J.C. Rodriguez-Aguilera, D.J.M. Fernandez-Ayala, G. Brea-Calvo, G. Lopez-Lluch, C. Santos-Ocana, Secondary CoQ10 deficiency, bioenergetics unbalance in disease and aging, Biofactors 47 (4) (2021) 551–569.
[24] R.M. Guerra, D.J. Pagliarini, Coenzyme Q biochemistry and biosynthesis, Trends Biochem. Sci. 48 (5) (2023) 463–476.
[25] W. Chen, D. Wang, L.S. Wang, D. Bei, J. Wang, W.A. See, S.R. Mallery, G.D. Stoner, Z. Liu, Pharmacokinetics of protocatechuic acid in mouse and its quantifica- tion in human plasma using LC-tandem mass spectrometry, J. Chromatogr. B Analyt. Technol. Biomed. Life Sci. 908 (2012) 39–44.
[26] J.A. Dominguez-Avila, A. Wall-Medrano, G.R. Velderrain-Rodriguez, C.O. Chen, N. J. Salazar-Lopez, M. Robles-Sanchez, G.A. Gonzalez-Aguilar, Gastro- intestinal interactions, absorption, splanchnic metabolism and pharmacokinetics of orally ingested phenolic compounds, Food Funct. 8 (1) (2017) 15–38.
[27] K.S. Echtay, E. Winkler, M. Klingenberg, Coenzyme Q is an obligatory cofactor for uncoupling protein function, Nature 408 (6812) (2000) 609–613.
[28] T.C. Esteves, K.S. Echtay, T. Jonassen, C.F. Clarke, M.D. Brand, Ubiquinone is not required for proton conductance by uncoupling protein 1 in yeast mitochondria, Biochem. J. 379 (Pt 2) (2004) 309–315.
[29] M. Jaburek, K.D. Garlid, Reconstitution of recombinant uncoupling proteins: UCP1, -2, and -3 have similar affinities for ATP and are unaffected by coenzyme Q10, J. Biol. Chem. 278 (28) (2003) 25825–25831.
[30] F.E. Sluse, W. Jarmuszkiewicz, R. Navet, P. Douette, G. Mathy, C.M. Sluse-Goffart, Mitochondrial UCPs: new insights into regulation and impact, Biochim. Biophys. Acta 1757 (5–6) (2006) 480–485.
[31] C.F. Chang, A.L. Gunawan, I. Liparulo, P.H. Zushin, A.M. Bertholet, Y. Kirichok, A. Stahl, CoQ regulates Brown adipose tissue respiration and uncoupling protein 1 expression, Antioxidants (Basel) 12 (1) (2022).
[32] D. Herebian, A. Seibt, S.H.J. Smits, R.J. Rodenburg, E. Mayatepek, F. Distelmaier, 4-Hydroxybenzoic acid restores CoQ(10) biosynthesis in human COQ2 deficiency, Ann. Clin. Transl. Neurol. 4 (12) (2017) 902–908.
[33] O.A. Nour, H.A. Ghoniem, M.A. Nader, G.M. Suddek, Impact of protocatechuic acid on high fat diet-induced metabolic syndrome sequelae in rats, Eur. J. Pharmacol. 907 (2021) 174257.
[34] S. Gabery, C.G. Salinas, S.J. Paulsen, J. Ahnfelt-Ronne, T. Alanentalo, A.F. Baquero, S.T. Buckley, E. Farkas, C. Fekete, K.S. Frederiksen, H.C.C. Helms, J.F. Jeppesen, L. M. John, C. Pyke, J. Nohr, T.T. Lu, J. Polex-Wolf, V. Prevot, K. Raun, L. Simonsen, G. Sun, A. Szilvasy-Szabo, H. Willenbrock, A. Secher, L.B. Knudsen, W.F. J. Hogendorf, Semaglutide lowers body weight in rodents via distributed neural pathways, JCI Insight 5 (6) (2020).
[35] M. Crestani, E. De Fabiani, D. Caruso, N. Mitro, F. Gilardi, A.B. Vigil Chacon, R. Patelli, C. Godio, G. Galli, LXR (liver X receptor) and HNF-4 (hepatocyte nuclear factor-4): key regulators in reverse cholesterol transport, Biochem. Soc. Trans. 32 (Pt 1) (2004) 92–96.
[36] L. Parlati, M. Regnier, H. Guillou, C. Postic, New targets for NAFLD, JHEP Rep 3 (6) (2021) 100346.
[37] V. Veeriah, S.H. Lee, F. Levine, Long-term oral administration of an HNF4- alpha agonist prevents weight gain and hepatic steatosis by promoting increased mitochondrial mass and function, Cell Death Dis. 13 (1) (2022) 89.
[38] A.P.G. da Silva, W.G. Sganzerla, O.D. John, R. Marchiosi, A comprehensive review of the classification, sources, biosynthesis, and biological properties of hydroxybenzoic and hydroxycinnamic acids, Phytochem. Rev. (2023).
[39] A. Teijeiro, A. Garrido, A. Ferre, C. Perna, N. Djouder, Inhibition of the IL-17A axis in adipocytes suppresses diet-induced obesity and metabolic disorders in mice, Nat. Metab. 3 (4) (2021) 496–512.
[40] G. Kleiner, E. Barca, M. Ziosi, V. Emmanuele, Y.M. Xu, A. Hidalgo-Gutierrez, C. H. Qiao, S. Tadesse, E. Area-Gomez, L.C. Lopez, C.M. Quinzii, CoQ(10) supplementation rescues nephrotic syndrome through normalization of H2S oxidation pathway, BBA-Mol. Basis Dis. 1864 (11) (2018) 3708–3722.
[41] M. Bakkali, R. Martin-Blazquez, RNA-Seq reveals large quantitative differences between the transcriptomes of outbreak and non-outbreak locusts, Sci. Rep. 8 (1) (2018) 9207.
[42] M.D. Robinson, D.J. McCarthy, G.K. Smyth, edgeR: a Bioconductor package for differential expression analysis of digital gene expression data, Bioinformatics 26 (1) (2010) 139–140.
[43] E.G. Bligh, W.J. Dyer, A rapid method of total lipid extraction and purification, Can. J. Biochem. Physiol. 37 (8) (1959) 911–917.
[44] C.A. Smith, E.J. Want, G. O'Maille, R. Abagyan, G. Siuzdak, XCMS: processing mass spectrometry data for metabolite profiling using nonlinear peak alignment, matching, and identification, Anal. Chem. 78 (3) (2006) 779–787.
[45] L. Garcia-Corzo, M. Luna-Sanchez, C. Doerrier, J.A. Garcia, A. Guaras, R. Acin-Perez, J. Bullejos-Peregrin, A. Lopez, G. Escames, J.A. Enriquez, D. Acuna-Castroviejo, L.C. Lopez, Dysfunctional Coq9 protein causes predominant encephalo- myopathy associated with CoQ deficiency, Hum. Mol. Genet. 22 (6) (2013) 1233–1248.